

Understanding summertime peroxyacetyl nitrate (PAN) formation and its relation to aerosol pollution: Insights from high-resolution measurements and modeling

Baoye Hu^{1,3,4}, Naihua Chen^{1,6}, Rui Li⁷, Mingqiang Huang^{1,3,4}, Jinsheng Chen^{2,5*}, Youwei Hong^{2,5}, Lingling Xu^{2,5}, Xiaolong Fan^{2,5}, Mengren Li^{2,5}, Lei Tong², Qiuping Zheng⁸, Yuxiang Yang^{6*}

¹College of Chemistry, Chemical Engineering and Environment, Minnan Normal University, Zhangzhou, China, 363000

²Center for Excellence in Regional Atmospheric Environment, Institute of Urban Environment, Chinese Academy of Sciences, Xiamen 361021, China

³Fujian Provincial Key Laboratory of Modern Analytical Science and Separation Technology, Minnan Normal University, Zhangzhou, China, 363000

⁴Fujian Province University Key Laboratory of Pollution Monitoring and Control, Minnan Normal University, Zhangzhou, China, 363000

⁵Fujian Key Laboratory of Atmospheric Ozone Pollution Prevention, Chinese Academy of Sciences, Xiamen 361021, China

⁶Pingtang Environmental Monitoring Center of Fujian, Pingtan 350400, China

⁷Key Laboratory of Geographic Information Science of the Ministry of Education, School of Geographic Science, East China Normal University, Shanghai 200241, PR China

⁸Xiamen Key Laboratory of Straits Meteorology, Xiamen Meteorological Bureau, Xiamen 361012, China

Correspondence to: Jinsheng Chen (jschen@iue.ac.cn) & Yuxiang Yang (907460293@qq.com)

Abstract: Peroxyacetyl nitrate (PAN), a key indicator of photochemical pollution, is generated similarly to ozone (O₃), through reactions involving specific volatile organic compounds (VOCs) and nitrogen oxides. Notably, PAN has been observed at unexpectedly high concentrations (maximum: 3.04 ppb) during the summertime. The daily maximum values of PAN showed a stronger correlation with black carbon (BC) (R=0.85) than with O₃ (R=0.75), suggesting a close connection between summertime haze and photochemical pollution. We addressed the puzzle of summertime PAN formation and its association with aerosol pollution under high O₃ conditions in Xiamen, a coastal city in southeastern China, by analyzing continuous high temporal resolution data utilizing box modeling in conjunction with the master chemical mechanism (MCM). The MCM model, with an index of agreement (IOA) value of 0.75, effectively investigate PAN formation, permorming better during the clean period (R²: 0.68, slope K: 0.91) than haze one (R²: 0.47, slope K: 0.75). Using extreme gradient boosting (XGBoost), we identified NH₃, NO₃, and PM_{2.5} as the primary factors for simulation bias. Moreover, the net production rate of PAN becomes negative with PAN constrained, suggesting

删除了: through a process

删除了: the photochemical reactions of

删除了: in the presence of

设置了格式: 下标

删除了: Notably, PAN has been observed at unexpectedly high concentrations (maximum: 3.04 ppb) during summertime that the daily maximum values of PAN were better correlated to black carbon (BC) (R²=0.85) than ozone (O₃) (R²=0.75), suggesting that summertime haze and photochemical pollution were deeply connected.

删除了: ozone

设置了格式: 下标

删除了: With

删除了: the MCM model proves to be an ideal tool for

删除了: investigating

删除了: photochemical

删除了: . The model performed

删除了: 6782

删除了: 9097

删除了: during the

删除了: period

删除了: 08

删除了: 7477

删除了: Through the machine learning method of

删除了: XGBoost

删除了: found

删除了: that the top three factors leading to simulation bias were

设置了格式: 上标

an unknown compensatory mechanism. Both [relative incremental reactivity \(RIR\)](#) and [empirical kinetic modeling approach \(EKMA\)](#) analyses indicate that PAN formation is VOC-controlled. Controlling emissions of VOCs, particularly alkenes, C₅H₈, and aromatics, would mitigate PAN pollution. PAN promotes OH and HO₂ while inhibiting the formation of O₃, RO₂, NO, and NO₂. This study deepens our comprehension of PAN photochemistry while also offering scientific insights for guiding future PAN pollution control strategies.

删除了: the existence of

删除了: in this region

删除了: RIR results also show that during the clean period, PAN is more sensitive to changes in various pollutants than during the haze period, underscoring the importance of deep emission reductions.

Introduction

PAN is a significant secondary gaseous pollutant commonly present in photochemical smog and poses risk to human health and plant growth, being 1-2 magnitudes more phytotoxic than O₃ (Yukihiro et al., 2012; Taylor, 1969). Additionally, PAN's low aqueous solubility, minimal reactivity with hydroxyl radicals (OH), and slow photolysis contribute to its capacity for long-range transport of nitrogen oxides (NO_x) (Xu et al., 2018; Zhai et al., 2024; Marley et al., 2007b). Therefore, its formation in polluted areas holds significant importance beyond local concerns. Similar to surface O₃, PAN is produced during the oxidation of VOCs in the presence of NO_x (R1-R3) (Xu et al., 2021). PAN is formed when NO₂ reacts with peroxyacetyl (PA) radicals (CH₃C(O)OO•) (R2), but the presence of NO consumes PA radicals, inhibiting PAN production (R3), which creates a comparable dependence of PAN and O₃ on NO and NO₂ levels. Unlike O₃, however, PAN is influenced by only a limited number of oxygenated VOCs (OVOCs) that generate PA radicals. These OVOCs, which are second-generation precursors of PAN, include acetaldehyde (CH₃CHO), acetone (CH₃C(O)CH₃), methylglyoxal (MGLY, CH₃C(O)CHO), methyl vinyl ketone (MVK, CH₂CHC(O)CH₃), methyl ethyl ketone (MEK, CH₃C(O)CH₂CH₃), methacrolein (MACR, CH₂C(CH₃)CHO), and biacetyl (CH₃C(O)C(O)CH₃). These compounds are typically formed from the oxidation of alkenes, aromatics, and isoprene, which are the first-generation precursors of PAN (Xue et al., 2014; Zhang et al., 2015). Identifying the dominant precursors is crucial for managing PAN pollution effectively. In the troposphere, thermal decomposition (R4) is the primary process responsible for PAN loss.

删除了: Peroxyacetyl nitrate (

删除了: , CH₃C(O)ONO₂)

删除了: ozone (

删除了:)

设置了格式: 下标

删除了: volatile organic compounds (

删除了:)

设置了格式: 字体: 非倾斜, 下标

删除了: (Xu et al., 2021)

删除了: (Xu et al., 2021)



In recent years, wintertime photochemical air pollution has increasingly garnered attention. At this time, the concentration of O₃ is low due to the strong titration of NO, while the concentration of aerosol is high, and it is found that aerosol promotes PAN generation (Xu et al., 2021). Surprisingly high concentrations of OH radical, particularly under hazy conditions, have been observed and are largely attributed to HONO photolysis (Xu et al., 2021). Winter photochemical and haze pollution often exacerbate each other, with photochemical trace gases supplying both oxidants and precursors for aerosol formation, and aerosols acting as mediums for

100 heterogeneous reactions that produce key oxidants such as HONO, H₂O₂, and OH radicals (Xu et al., 2021). The OH produced by
101 HONO photolysis can partially replace the UV action to promote PAN formation in winter in southeast coastal area of China when
102 particulate matter is high ($\geq 35\mu\text{g}\cdot\text{m}^{-3}$) (Hu et al., 2020). Zhang et al. (2020) found the potential HONO sources significantly
103 improved the PAN simulations in wintertime heavy haze events with high concentrations of PAN. High concentrations of PAN are
104 a consequence of the increased levels of precursors and HONO observed during haze episodes (Liu et al., 2018). In conclusion,
105 most previous studies have studied the effect of aerosol on PAN generation in winter. Further research on PAN should determine
106 whether particulates significantly contribute to its formation during warmer seasons with elevated O₃ concentrations (Xu et al.,
107 2021). In Eastern China, photochemical air pollution often involves high concentrations of both O₃ and PAN, a persistent issue
108 during the warm season (April-September) for many years (Lu et al., 2020). The characteristics and formation pathways of PAN
109 during summer have been increasingly studied in regions such as the North China Plain (NCP), the Yangtze River Delta, the Pearl
110 River Delta, and southwestern China. These studies have generally shown consistent diurnal patterns and strong correlations
111 between PAN and O₃, identifying acetaldehyde—primarily derived from the degradation of aromatics and alkenes—as the key direct
112 precursor of PAN in the summer. However, there has been limited research on the formation of PAN and its relationship with aerosol
113 pollution during the summertime.

114 Xiamen is one of the fastest urbanizing regions in the southeast China and is also one of the cities with the best air quality in China,
115 where the air quality could represent the future of other Chinese urban regions. Between 2018 and 2023, Xiamen ranked among the
116 top 10 cities in China, achieving positions of 7th in 2018, 4th in both 2019 and 2020, 6th in 2021, 9th in 2022, and returning to 7th
117 in 2023 (mee.gov.cn, last assessed October 30, 2014). Xiamen is located in a low-latitude coastal area, with abundant sunlight and
118 long daylight hours during the summer, resulting in strong solar radiation and rapid photochemical conversion rates. The city is
119 typically influenced by the East Asian monsoon and serves as a transport channel for atmospheric pollutants from both the Yangtze
120 River Delta and Pearl River Delta regions. Additionally, during the summer, Xiamen is often affected by complex meteorological
121 conditions such as typhoons and the West Pacific Subtropical High (WPSH). The WPSH creates weather conditions that promote
122 the formation and accumulation of photochemical pollutants and particulate matter (Wu et al., 2019). This setting provides an ideal
123 "laboratory" for investigating the complexities of summertime PAN formation and its relationship with aerosol pollution under high
124 O₃ concentrations. In summer, especially in July, high temperatures, high humidity, and intense radiation are likely to accelerate
125 both the formation and consumption rates of PAN. In this study, continuous measurements of trace gases, substances related to
126 aerosols, photolysis rate constants and meteorological parameters were performed at a suburban site in Xiamen from July 10th to
127 July 31st, 2018. Firstly, we provide an overview of pollutant concentrations, meteorological parameters, and weather conditions
128 during the observation period. Secondly, we simulate PAN concentration with the aid of box modeling combined with master
129 chemical mechanism (MCM). Using machine learning with XGBoost, we identified the key factors that affect the observation-based
130 model (OBM) model's simulation results and clarified the mechanisms linking haze pollution to photochemical air pollution, as

删除了: ozone

设置了格式: 下标

删除了: peroxyacetyl nitrate (

删除了:)

删除了: Xiamen is also often affected by typhoons and subtropical weather forms in summer

删除了: West Pacific Subtropical High (

删除了:)

删除了: ozone

设置了格式: 下标

139 indicated by PAN and O₃. Thirdly, the study identified the main precursors and oxidants responsible for summertime PAN production
140 in Xiamen and evaluated the influence of PAN on local atmospheric oxidation capacity. This study further emphasized the interplay
141 between haze and photochemical air pollution and highlighted significant implications for future research.
142

删除了: Using a machine learning-XGBoost looks for the key factors that affect the model's simulation result and clarified the mechanisms linking haze pollution to photochemical air pollution, as indicated by PAN and O₃.
设置了格式: 下标

143 2 Methodology

144 2.1 Field observations

145 Trace gases (including PAN, O₃, HONO, HNO₃, HCl, NH₃, VOCs, NO_x, CO, and SO₂), substances related to aerosols (including
146 BC, PM₁, PM_{2.5}, PM₁₀, SO₄²⁻, NO₃⁻, NH₄⁺, Cl⁻, Na⁺, K⁺, Ca²⁺, Mg²⁺), photolysis rate constants (including JO¹D, JNO₂, JHONO,
147 JHCHO_M, JHCHO_R, JNO₃_M, JNO₃_R, JH₂O₂), and meteorological parameters (including temperature, relative humidity,
148 atmospheric pressure, wind speed, and wind direction) were continuously measured at a suburban site in Xiamen from July 10th
149 to July 31st, 2018. All instruments were placed inside an air-conditioned container situated on the rooftop of a 20-story building at
150 the Institute of Urban Environment, Chinese Academy of Sciences (IUE: 118.06°E, 24.61°N) (Fig. S1(a)). When southerly winds
151 prevailed, Xiamen Island, characterized by dense population and traffic congestion, was located upwind of the IUE (Fig. S1(b)).
152 The IUE supersite is surrounded by Xinglin Bay, several universities and institutes, and major roadways with heavy traffic, such as
153 Jimei Road (< 200 m), Shenhai Expressway (870 m), and Xiasha Expressway (2300 m) (Fig. S1(c)).

设置了格式: 字体: 非倾斜, 下标

154 PAN measurements were conducted using a PANS-1000 analyzer (Focused Photonics Inc., Hangzhou, China), which features an
155 automated system consists of a gas chromatograph, an electron capture detector, and a calibration unit. The analyzer provided PAN
156 readings every 5 minutes, with a detection limit of 50 ppt. The uncertainty and precision of the PAN measurements were ±10% and
157 3%, respectively. The PAN standard gas was produced through the reaction of acetone and NO under UV light. Calibration
158 procedures included monthly multi-point calibrations and weekly single-point calibrations. Detailed information about the PAN
159 detection system and calibration can be found in previous studies (Hu et al., 2020; Liu et al., 2022a). The VOC measurements were
160 conducted using a gas chromatography mass spectrometer (GC-FID/MS, TH-300B, Wuhan, China) at an hourly time resolution.
161 Detailed information regarding the VOC detection system and calibration procedures is available in our previous study (Liu et al.,
162 2022b). HONO measurements were conducted using a customized Incoherent BroadBand Cavity Enhanced Absorption
163 Spectroscopy (IBBCEAS) system developed by the Anhui Institute of Optics and Fine Mechanics (AIOFM), Chinese Academy of
164 Sciences. The HONO detection limit was 100 ppt, with a time resolution of 1 minute. The measurement principle and calibration
165 method of IBBCEAS can be found in the previous literature (Hu et al., 2022; Duan et al., 2018; Hu et al., 2024). The concentrations
166 of inorganic components in PM_{2.5} aerosols (including SO₄²⁻, NO₃⁻, NH₄⁺, Cl⁻, Na⁺, K⁺, Ca²⁺, Mg²⁺), as well as the concentrations of
167 gases such as NH₃, HCl, and HNO₃ were analyzed using a Monitor for AeRosols and Gases in ambient Air (MARGA, Model ADI
168 2080, Applikon Analytical B.V., the Netherlands) (Hu et al., 2022). The criteria air pollutants O₃, NO_x, CO, and SO₂ were measured
169 using different methods: ultraviolet (UV) absorption for O₃ (TEI model 49i), chemiluminescence with a molybdenum converter for

设置了格式: 字体: 非倾斜, 下标

174 NO_x (TEI model 42i), non-dispersive infrared for CO (TEI model 48i), and pulsed UV fluorescence for SO₂ (TEI model 43i). A
175 tapered element oscillating microbalance (TEOM1405, Thermo Scientific Corp., MA, USA) was used to continuously measure the
176 mass concentrations of PM₁, PM_{2.5}, and PM₁₀ online. A photolysis spectrometer (PFS-100, Focused Photonics Inc., Hangzhou,
177 China) was employed to measure the photolysis rate constants. An ultrasonic anemometer (150WX, Airmar, USA) was used to
178 measure meteorological parameters.

设置了格式: 字体: 非倾斜, 下标

180 2.2 Box modeling

181 This study employed a box model framework utilizing the Master Chemical Mechanism (MCMv3.3.1,
182 <https://mcm.york.ac.uk/MCM/home.htm>) to investigate sensitivity and mechanisms of PAN formation. The model constraints were
183 derived from observations of trace gases and meteorological parameters, which were averaged to 1-hour intervals. The reliability of
184 model simulation results is often assessed using the index of agreement (IOA), which ranges from 0 to 1, with a higher IOA
185 signifying greater alignment between observed and simulated values. Note that the model simulation values at this time are not
186 constrained by PAN. For specific formulas, please refer to the supplementary information (Eq. S1). Other formulas, including PAN
187 production rates (P(PAN)), net production of PAN (Net (PAN)), and the RIR_x are provided in the supplementary information (Eq.
188 S2- Eq. S4).

删除了: relative incremental reactivity (

删除了:)

189 The MCM simulates the nonlinear interaction between PAN and its precursors by altering the VOCs-to-NO_x ratio across multiple
190 scenarios, while keeping all other parameters fixed. In this study, a 20% step size was applied, reducing VOCs and NO_x from 200%
191 down to 0% to construct a scenario matrix. A total of 121 scenarios were generated to model the PAN production rate. The scenario
192 representing the average VOCs and NO_x mixing ratio during the sampling period was designated as the base case, with the remaining
193 120 scenarios created by systematically adjusting the VOC-to-NO_x ratio. The output from these 121 simulations was used to
194 construct isopleth diagrams depicting the relationship between VOCs, NO_x, and PAN.

设置了格式: 下标

设置了格式: 下标

设置了格式: 下标

设置了格式: 下标

设置了格式: 下标

195 2.3 Machine Learning Model

196 To identify the key factors influencing the performance of the model simulation, the Machine Learning (ML) model was applied to
197 establish the prediction model of bias between simulation of OBM and observation. XGBoost is a supervised boosting algorithm
198 that reduces the risk of over-fitting, captures the nonlinear relationships among predictor variables, and solves numerous data science
199 problems in a rapid and accurate way (Li et al., 2024). It has demonstrated high performance in O₃ studies in over China. As
200 compared to other bagging tree models like random forest, XGBoost can handle more complex data while consuming fewer
201 computing resources. To further improve the interpretability of the ML model, the feature importance of independent input variables
202 in the XGBoost model is quantified using the Shaply Additive explanation (SHAP) approach (Lin et al., 2024). The SHAP calculates
203 a value that represents the contribution of each feature to the model's outcome, which has been successfully applied in atmospheric
204 environmental studies (Li et al., 2024; Lin et al., 2024). When the model was being adjusted, 90% of the data was used as the training

删除了: OBM

删除了: '

209 set, and 10% of the data was used as the test set. The hyperparameters were tuned using grid search and cross-validation method.
210 Specifically, for a single hyperparameter, grid search was used to obtain its more appropriate value range, and for the combinations
211 of hyperparameters, the whole training set was split into ten folds and then run a grid search over pre-adjusted combinations of
212 hyperparameters by training nine folds and predicting on the one fold in cross-validation procedure. For key hyperparameters of
213 XGBoost model, the number of trees was 100, learning rate was 0.1, max depth was 6. The model was trained and tested on hourly
214 data during the whole observation and the established model was examined by coefficient of determination (R^2) value, the root-
215 mean-squared error (RMSE) and mean absolute error (MAE). The formulas of RMSE and MAE are provided in the supplementary
216 information (Eq. S5 & Eq. S6). The performance of both models is illustrated in Fig. S3. The R^2 , MAE, and RMSE for the training
217 set are 0.90, 0.08, and 0.12, respectively, while the corresponding values for the test set are 0.77, 0.10, and 0.14, respectively. These
218 statistical metrics indicate that the XGBoost model is promising for further analysis.

删除了: '
删除了: 37
删除了: 7664

220 3. Results and discussion

221 3.1 Overview of observation

222 The measured data of PAN, related trace gases and meteorological parameters at IUE over 10-31 July 2018 are documented in Fig.
223 1. Combined with the synoptic situation shown in Fig. S4, the 8th typhoon of 2018, Typhoon Maria, made landfall on the morning
224 of the 11th at Huangqi Peninsula in Lianjiang County, Fujian. Due to the influence of the typhoon's outer spiral rain bands, there
225 was moderate to heavy rain on the 11th. Correspondingly, there was a noticeable decrease in ultraviolet radiation and the
226 temperatures. Starting from the 12th, a WPSH strengthened and extended westward, exerting control over Xiamen. In the lower
227 atmosphere, it was influenced by the eastward flow, resulting in predominantly cloudy weather. From the 16th to the 18th, the area
228 was affected by the outer periphery of Typhoon Shan Shen, which formed on the 17th in the northeastern part of the South China
229 Sea and moved westward, making landfall along the coast of Wancheng Town, Wanning City, Hainan Province in the early hours
230 of the 18th. During this period, the city experienced strong winds with gusts reaching 5 to 6 on the Beaufort scale in the urban areas.
231 At the same time, the concentration of various pollutants reached their lowest levels, and the daily variation patterns were less
232 pronounced. From the 20th to the 21st, Xiamen experienced the influence of the peripheral descending airflow associated with
233 Typhoon Ampil (which formed in the northwest Pacific Ocean around 8:00 P.M. on the 18th and moved northwest, making landfall
234 along the coast of Chongming Island, Shanghai, around noon on the 22nd). During this period, there were fewer clouds and higher
235 temperatures. From the 22nd to the 24th, the city was successively affected by the outer periphery of Typhoon Ampil and a tropical
236 low-pressure system, resulting in occasional showers or thunderstorms. From the 25th to the 31st, a WPSH once again strengthened
237 and controlled Xiamen. As a result, Xiamen experienced stable meteorological conditions, with light winds ($w_s = 1.04 \text{ m/s}$),
238 persistently high temperatures (maximum daily average of 37.82°C), and high relative humidity (maximum daily average of
239 81.65%). These factors created an environment that favored the buildup of particulate matter and enhanced the photochemical

删除了: Combine with the synoptic situation (Fig. S4), the 8th typhoon of 2018, Typhoon Maria, made landfall on the morning of the 11th in Huangqi Peninsula, Lianjiang County, Fujian...
删除了: Western Pacific subtropical high (
删除了:)
删除了: city

删除了: City

删除了: City
删除了: city
删除了: /
删除了: daily maximum average
删除了: daily maximum average

256
257
258
259
260
261
262
263
264
265
266
267
268
269
270
271
272

formation of O₃ and PAN (Wu et al., 2019). The maximum daily average of PM_{2.5}, O₃ and PAN were 49.26 μg·m⁻³, 93.62 ppb, and 1.37 ppb, respectively.

The phenomenon of simultaneous high levels of photochemical and particulate matter appears. Throughout the 22-days campaign, 12 days (including July 11th, 13th, 21st to 23rd, and 25th to 31st) were observed with 1 h concentrations of PM_{2.5} exceeding 35 μg·m⁻³; 13 days (including July 11th, 13th, 15th, 20th to 23rd, and 26th to 31st) were observed with 5-min concentrations of PAN exceeding 1 ppb. The maximum concentration was recorded at 3.04 ppb (5-min data) at 11:09 local time of 13 July 2018. This concentration of PAN is comparable to the levels recorded at downwind of Guangzhou, southern China (3.9 ppb) (Wang et al., 2010), 2.51 ppb in Nashville, U.S (Roberts et al., 2002). However, this value was significantly lower than heavily polluted areas in northern China in the summer, such as Beijing (9.34 ppb, (Xue et al., 2014)), Lanzhou (9.12 ppb, (Zhang et al., 2009)), and Jinan (13.47 ppb, (Liu et al., 2018)). This is likely because the higher summer temperatures in the southeastern coastal region are conducive to the thermal decomposition of PAN, and the precursor concentrations of PAN, including NO₂ and VOCs, are significantly lower in the studied area compared to those in the northern region. The concentration of alkanes is the highest, followed by alkenes, OVOCs and aromatics, while halogenated hydrocarbons and C₆H₆ exhibit lower concentrations (Fig. S5). Furthermore, VOC concentrations for various species are elevated during haze periods compared to clean periods (Fig. S5). Throughout the observation period, the variations in O₃ and PAN were almost identical, but the maximum concentration of O₃ occurred at 3:00 p.m. on July 29th (114.12 ppb). The correlation between the maximum daily values of PAN and BC is the strongest (R=0.85), followed by O₃ (R=0.75) (Fig. S6), suggesting that summertime haze and photochemical pollution were deeply connected.

删除了: daily maximum average

设置了格式: 下标

删除了: the precursor concentration of PAN is significantly lower than in the northern region

设置了格式: 下标

设置了格式: 下标

删除了: maximum

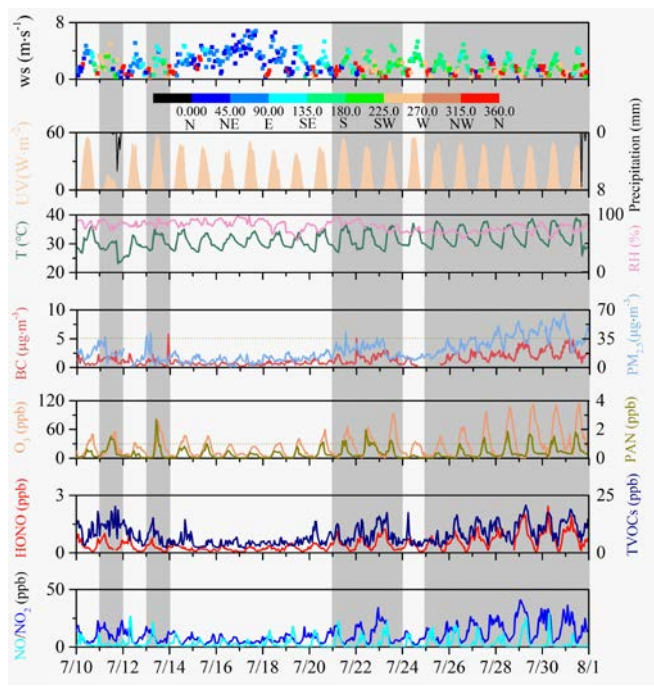
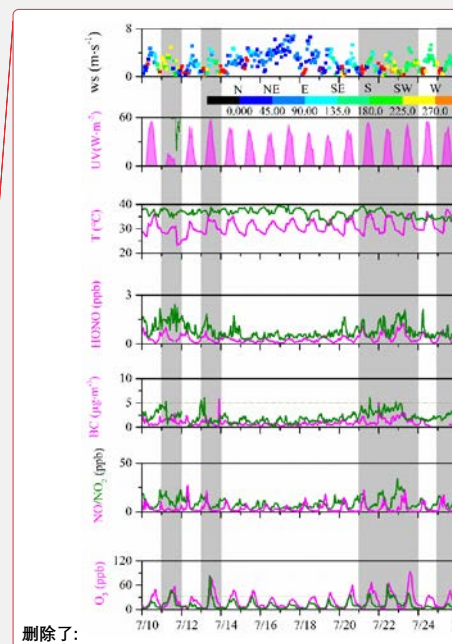


Figure 1. Time series of trace gases and meteorological parameters observed at IUE during 10-31 July 2018. The gray shading represents days when the $PM_{2.5}$ hourly daily maximum value exceeded $35 \mu\text{g}\cdot\text{m}^{-3}$.

We categorize it as "haze" and "clean" based on whether the $PM_{2.5}$ hourly daily maximum value is greater than $35 \mu\text{g}\cdot\text{m}^{-3}$. Specifically, "haze" includes July 11th, 13th, 21st to 23rd, and 25th to 31st, while other days are categorized as 'clean'. To provide a quantitative perspective, the statistics for PAN and associated species were calculated and compiled in Table 1. $PM_{2.5}$ concentrations during the haze period were significantly higher than those during the clean period, being 2.49 times those of the clean period. There was no significant difference of UV levels between clean and haze periods, while temperatures in the haze phase were notably higher than those in the clean phase. Therefore, without considering precursors, PAN concentrations should be lower during the haze phase due to higher thermal decomposition. In fact, PAN concentrations during the haze period were 2.35 times higher than those during the clean period. During the haze period, O_3 concentrations were also significantly higher than those during the clean period, being 2.04 times those of the clean period. These observations indicate that the atmospheric oxidation capacity is relatively strong during the haze period. Similar to PAN, HONO also exhibits higher concentrations during the haze phase (approximately 2.33 times that of clean conditions), which is consistent with current research findings that particles promote the generation of HONO (Ye et al., 2017). NO also experienced an increase from clean (3.28 ppb) to hazy (4.30 ppb) conditions, albeit less prominently than NO_2 (from 7.21 to 14.55 ppb). This observation further underscores that, during hazy periods, the



删除了:

删除了: 设置了格式: 下标

删除了: $PM_{2.5}$ concentrations during the haze period were significantly higher than during the clean period, being 2.49 times that of the clean period

删除了: 设置了格式: 下标

删除了: During the haze period, ozone concentrations were also significantly higher than during the clean period, being 2.04 times that of the clean period

301 atmosphere demonstrates heightened oxidizing potential, facilitating the conversion of NO to NO₂. While the increased NO levels
 302 on hazy days reduced PA radicals and hindered PAN formation, this effect was offset by the concurrently higher concentrations of
 303 PAN precursors (NO₂ and VOCs) during those days. The TVOCs have increased to some extent, but in hazy conditions, they are
 304 only 1.34 times that of clean conditions. This is also because the strong oxidizing conditions during haze periods convert VOCs
 305 into secondary pollutants, such as O₃ and PAN. Although it is acknowledged that VOCs can also be converted into secondary
 306 organic aerosol (SOA), the discussion of SOA is beyond the scope of this study. The TVOC levels at this site are comparable to
 307 that at a rural site in a coastal city-Qingdao (7.6 ppb), significantly lower than inland sites (such as Wuhan (30.2, (Liu et al., 2021a))
 308 and Chengdu (28.0 ppb, (Yang et al., 2020))) or economically more developed coastal cities (such as Shanghai (25.3 ppb, (Zhu et
 309 al., 2020)) and Hong Kong (26.9, (Wang et al., 2018))), and significantly higher than regional background locations like Mt. Wuyi
 310 (4.7 ppb, (Hong et al., 2019)), and Mt. Nanling (4.7 ppb, (Wang et al., 2023)), and global background station Mt. Waliguan (2.6
 311 ppb, (Xue et al., 2013)). The isoprene level during haze period was significantly higher than that during clean period probably due
 312 to haze period with higher temperature (Wang et al., 2023). The wind speed was very low during both the clean and haze periods,
 313 especially during the haze period with only 1.12 m·s⁻¹. The relative humidity was high during both periods, and there was no
 314 significant difference between the clean and haze periods.

315 **Table 1.** Descriptive statistics of major trace gases (ppb), particulate matter (μg·m⁻³) and meteorological parameters during 10-31
 316 July 2018.

Species	Clean (mean ± SD)	Haze (mean ± SD)
PAN	0.20 ± 0.23	0.47 ± 0.46***
O ₃	16.07 ± 12.73	32.79 ± 29.73***
HONO	0.27 ± 0.18	0.63 ± 0.43***
NO	3.28 ± 4.03	4.30 ± 8.39***
NO ₂	7.21 ± 3.87	14.55 ± 8.89***
TVOCs	6.13 ± 1.73	8.19 ± 2.55***
C ₅ H ₈	0.13 ± 0.04	0.17 ± 0.05***
PM ₁	10.13 ± 3.91	24.36 ± 10.77***
PM _{2.5}	11.21 ± 5.33	27.93 ± 13.16***
PM ₁₀	24.26 ± 9.45	47.28 ± 20.63***
UV (W·m ⁻²)	14.29 ± 17.38	13.18 ± 17.40
T (°C)	30.68 ± 2.39	31.92 ± 3.36***
RH (%)	81.94 ± 8.60	77.18 ± 8.22
WS (m·s ⁻¹)	1.64 ± 0.69	1.12 ± 0.61*

317 Note: *, **, and *** indicate that they passed the significance test at 0.05, 0.01 and 0.001 levels, respectively.

318 The average diurnal patterns of PAN and related variables have been averaged separately for clean and hazy conditions (Fig. 2).

320 The daily variation of PAN exhibits a clear unimodal pattern, with concentrations starting to rise after sunrise and decreasing after

下移了 [1]: Mt. Waliguan (2.6 ppb, (Xue et al., 2013)),

移动了(插入) [1]

删除了:),

删除了:),

删除了: .

删除了: .

325 12:00 caused by thermal decomposition of PAN at high temperatures (Fig. 2). Although PAN and O₃ exhibit a slight bimodal
327 pattern during the clean period, this is primarily due to the bimodal pattern of UV during this time. The peak occurring at noon
328 indicates that PAN primarily originates locally, as a delay of about 1-2 hours would be expected if it were influenced by
329 transportation (Liu et al., 2024). The daytime increment was much larger for hazy condition (1.17 ± 0.44 ppb) than for clean
330 condition (0.52 ± 0.21 ppb), indicating stronger photochemical production of PAN for hazy condition. The daily variation pattern
331 of O₃ is similar to PAN, except that O₃ reaches its peak relatively later compared to PAN, with the peak occurring at 16:00 during
332 the clean phase and 14:00 during the haze phase. Although PAN and O₃ are both products of photochemical reactions involving
333 NO_x and VOCs, their production efficiencies differ. PAN is specifically formed from VOCs that are precursors to the acetyl radical
334 (CH₃CO), whereas O₃ can be produced from the oxidation of any VOCs. Analyzing the correlation between PAN and O₃ can offer
335 insights into their respective photochemical production efficiencies. As shown in Fig. S7, the positive correlation between the daily
336 maximum values of PAN and O₃ for clean condition (R²=0.6701) was better than that for hazy condition (R²=0.1504). The slopes
337 of the linear regression were 0.021 ppb/ppb for clean conditions and 0.009 ppb/ppb for hazy conditions. This indicates that, on
338 average, approximately 2.1 ppb of PAN could be produced for each 100 ppb of O₃ formed under clean conditions, and about 0.9
339 ppb of PAN for each 100 ppb of O₃ under hazy conditions in the air masses reaching IUE. The slope of linear regression for clean
340 condition is comparable to those determined in Hongkong (0.028, (Xu et al., 2015)), Mexico city (0.02, (Marley et al., 2007a)),
341 and Nashville (0.025, (Roberts et al., 2002)). The lower efficiency of PAN production relative to O₃ indicates that PAN precursors
342 represent only a small portion of the total VOCs, especially during hazy conditions. Additionally, the high temperatures in the
343 southeast coastal region likely contribute to the lower production efficiency of PAN. The average temperature during the entire
344 observation period was 31.39 °C, with an average temperature of 34.64 °C at 12:00 LT. This result is consistent with the result that
345 RIR during the cleaning period is higher than that during the haze period. As shown in Fig. S8, in the clean period, the correlation
346 between PAN and O₃ is the strongest (R²=0.70), indicating that O₃ and PAN are both photochemical end products during clean
347 periods. In contrast, during hazy periods, the correlation between PAN and O₃×JO¹D is the strongest (R²=0.66), suggesting that
348 O₃ plays a more significant role in promoting PAN formation through photolysis to generate OH during hazy periods.
349 Unlike the daily variation patterns of PAN and O₃, HONO exhibits a swift concentration decrease after sunrise in both clean and
350 hazy conditions, undergoing photolytic conversion into OH radicals. Subsequently, in clean conditions, HONO starts to increase
351 in concentration after sunset. In hazy conditions, however, the increase begins from 16:00 LT and not after sunrise. This suggests
352 a robust daytime net production or transport of HONO, where the rates surpass those of HONO photolysis and other sinks in the
353 afternoon in hazy conditions. The NO levels reach their peak at 7:00 during the morning rush hour, reflecting advection of fresh
354 urban plumes to the study site. The daily variation of NO₂ exhibits a 'U' shape, reaching its minimum value at 13:00, mainly owing
355 to effects of emission, boundary layer height and photochemical reactions. In the clean period, the daily variation of PM_{2.5} is
356 similar to that of NO₂, both showing a 'U' shape, reaching their lowest values at noon. However, during the haze phase, the daily

设置了格式: 下标

删除了: ozone

删除了: ozone

设置了格式: 下标

设置了格式: 下标

设置了格式: 字体: 非倾斜, 下标

删除了: S5

删除了: S6

删除了: 42

删除了: 6597

variation pattern of PM_{2.5} appears somewhat different. There is a noticeable trough in the early morning, remains stable during the day, and starts to rise after sunset. The diurnal variation of VOC concentrations for various species are not significant during clean periods (Fig. 2(e)), likely due to higher wind speeds that facilitate the dispersion of pollutants. In contrast, during haze periods, the daily variations are evident, with peaks occurring before sunrise, followed by a decline, and then an increase after sunset (Fig. 2(f)). This is because the haze period is relatively stable at nighttime, which allows for the accumulation of pollutants, while during the daytime, sunlight converts VOCs into photochemical products like O₃ and PAN.

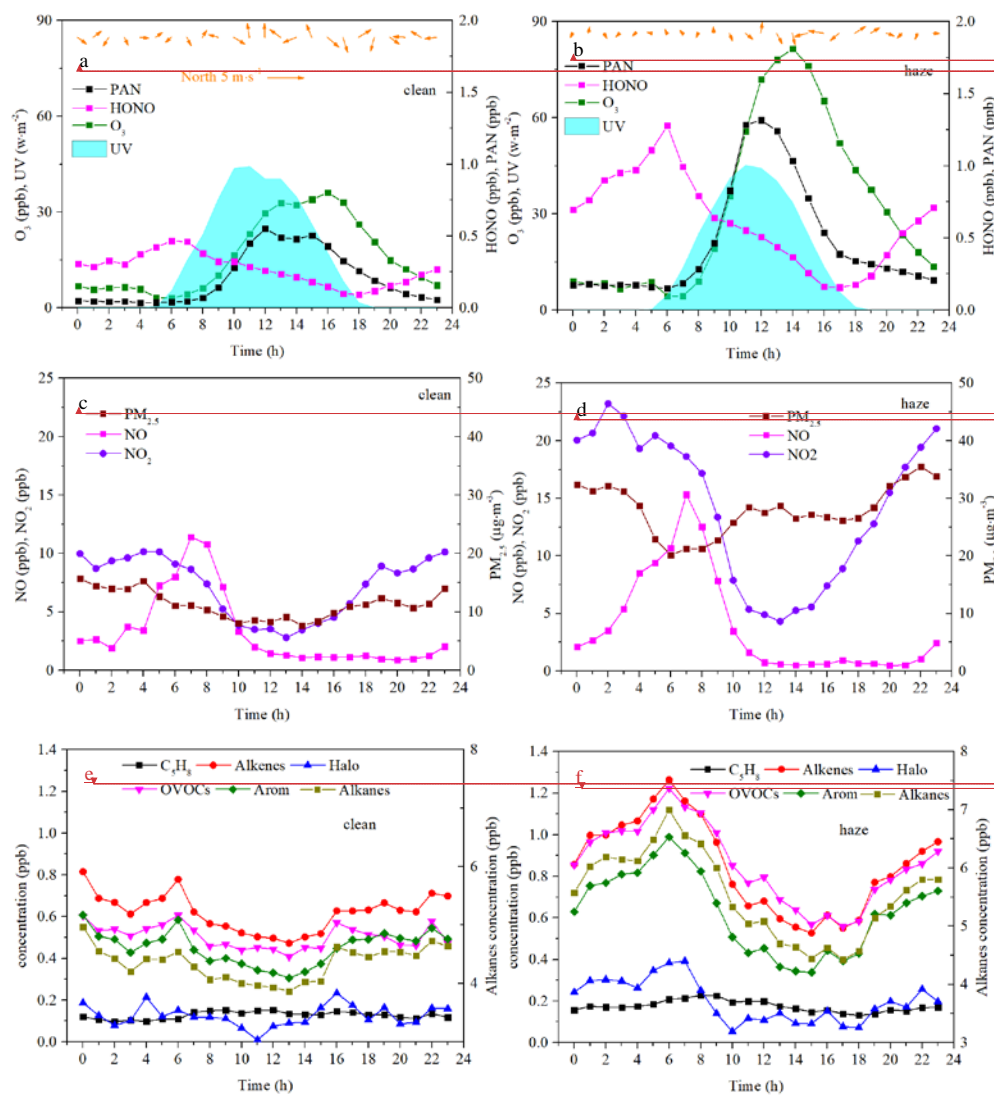


Figure 2. The diurnal variations of PAN, HONO, O₃, and UV during clean (a) and hazy (b) periods, the diurnal variations of PM_{2.5},

设置了格式: 下标

设置了格式: 字体: 五号

设置了格式: 字体: 五号

设置了格式: 字体: 五号

设置了格式: 字体: 五号

删除了: c

删除了: c

删除了: as well as

NO, and NO₂ during clean (c) and hazy (d) periods, and the diurnal variations of isoprene (C₅H₈), Alkenes, halogenated hydrocarbons (Halo), OVOCs, aromatics (Arom), and alkanes during clean (e) and hazy periods (f).

3.2 PAN formation: key factors and mechanisms

To investigate the key factors and mechanisms of PAN formation, PAN was simulated by constraining the MCM-based box model with meteorological conditions and observed concentrations of precursor gases. The model successfully replicated the variations in PAN, achieving an IOA of 0.75. (Fig. 3(a)), which was within the accepted range (0.66-0.87) in previous studies (Zeng et al., 2019). The model captured its formation rate well in general, with observed rates varying from 0.04 to 0.52 ppb·h⁻¹ (average: 0.20 ppb·h⁻¹) and modeled rates ranging from 0.09 to 0.46 ppb·h⁻¹ (average: 0.19 ppb·h⁻¹) (see Fig. 3(b)). The similar result was found in the North China Plain (NCP) region in the wintertime (Xu et al., 2021). When calculating the IOA separately for clean and hazy periods, it was found that the IOA significantly increased to 0.89 and 0.81 (Fig. 3(c)), respectively. This phenomenon indicates a substantial difference in the PAN production and destruction mechanisms between clean and hazy periods. Furthermore, the simulated values are closer to the observed values during clean period, reflected in a higher R² value (R²=0.68) and a slope value (K) closer to 1 (K=0.91) (Fig. 3(c)). In contrast, the R² value and the K value during hazy period are only 0.47 and 0.75, respectively (Fig. 3(c)). This phenomenon suggests that some reactions related to PAN generation or destruction might be missing in the MCM during the hazy period.

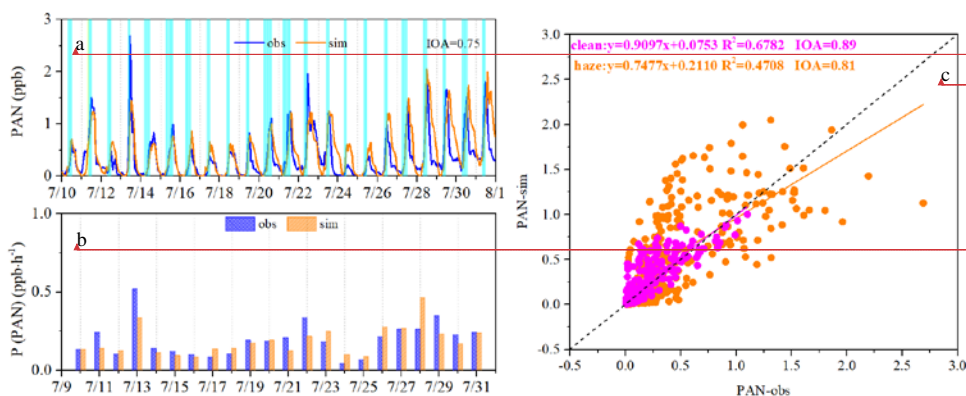


Figure 3. Comparisons of observed (obs) PAN and simulated (sim) PAN (daytime photochemical PAN production periods indicated by cyan shading), (b) production rates, (c) correlation between PAN observations and simulated values.

To identify the key factors influencing the performance of the OBM model simulation, the bias (the model simulation minus the observed value) as the target. The remaining variables, which were not input into the OBM model, such as NH₃, HNO₃, HCl (alkaline and acidic gaseous pollutants), PM_{2.5} concentrations and their components, as well as physical process parameters like

设置了格式: 下标

设置了格式: 下标

删除了: .

删除了: 6782

删除了: K

删除了: 9097

删除了: 08

删除了: 7477

删除了: reactions without considered in MCM may enhance PAN generation during hazy periods

删除了:

设置了格式: 字体: 五号

设置了格式: 字体: 五号

设置了格式: 字体: 五号

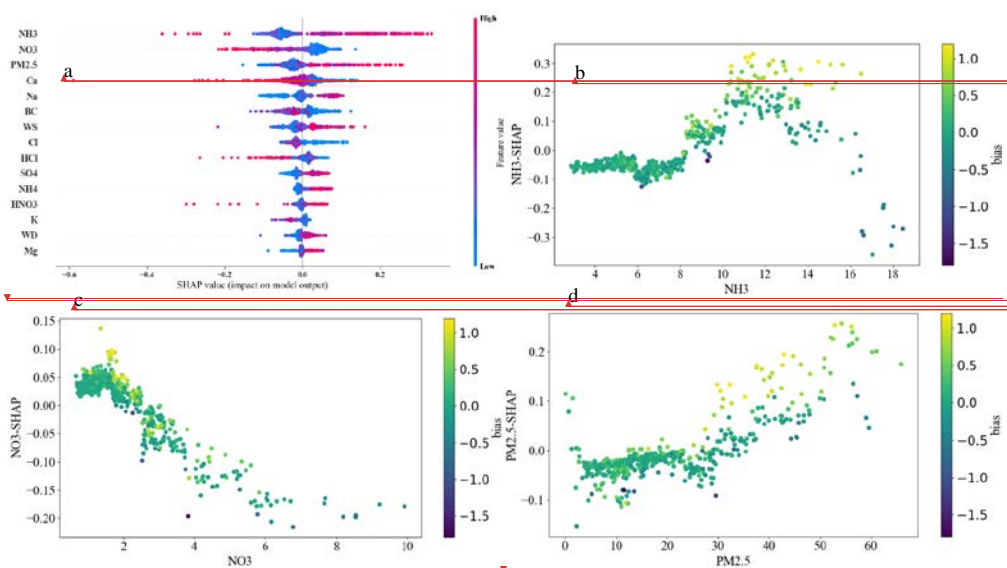
删除了: modeled PAN and observed PAN (a) variation

删除了:

删除了: we used the difference between the model simulation values and the observed values

删除了: (bias)

411 wind speed and wind direction, were used as features. As shown in Fig. 4 (a), through XGBoost-SHAP machine learning, we found
 412 that NH₃ is the most significant parameter affecting bias, contributing 19.68 % (Fig. S9). A scatter plot analysis of the SHAP values
 413 of NH₃ versus NH₃ concentrations revealed that as NH₃ concentrations increase (Fig. 4 (b)), the OBM model tends to overestimate
 414 more significantly. To date, there are very few studies that directly address the impact of NH₃ on PAN formation. Xu et al. (2021)
 415 suggested that NH₃ could promote the formation of HONO, which in turn affects PAN formation. However, since we included
 416 HONO as an input to constrain the model, the indirect influence of NH₃ on PAN formation through HONO can be excluded. NH₃
 417 in the atmosphere can preferentially react with sulfuric acid (H₂SO₄) to form ammonium sulfate ((NH₄)₂SO₄) secondary inorganic
 418 aerosols (Behera et al., 2013), leading to the heterogeneous reaction removal of PAN by secondary inorganic aerosols (Pratap et
 419 al., 2021). This result is validated by the positive correlation between the SHAP values of NH₄⁺ and SO₄²⁻ and their respective
 420 concentrations (Fig. S10). NO₃⁻ is the second most significant parameter influencing the bias between the two, contributing 11.33 %
 421 ((Fig. S9)). NO₃⁻ has a negative correlation with the bias (Fig. 4 (c)), indicating that higher NO₃⁻ levels lead to more significant
 422 underestimation by the model. Considering the significant positive correlation between PAN and NO₃⁻ at the 0.01 level, with a
 423 correlation coefficient of 0.37, and the fact that both reach their peaks around noon (Fig. S11), it is likely that they have a common
 424 source. PM_{2.5} is the third most significant parameter (Fig. 4 (a)), contributing 9.40 % (Fig. S9). PM_{2.5} has a positive correlation
 425 with the bias (Fig. 4 (d)), indicating that higher PM_{2.5} levels lead to more significant overestimation by the model, suggesting that
 426 PAN can undergo heterogeneous removal on the surface of PM_{2.5} in the actual atmosphere (Sun et al., 2022).



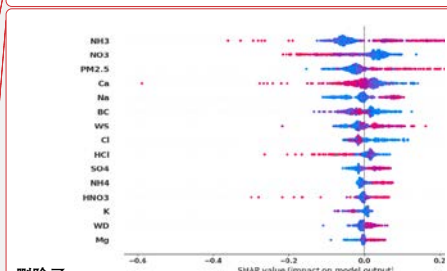
427 **Figure 4.** Feature importance was obtained by XGBoost-SHAP method (a). The scatter plots between concentration of top three
 428 important features and their SHAP values (b, c and d), and colored with the bias (the model simulation minus the observed value),
 429
 430
 431

删除了: negative

删除了: Fig. 4 (a)

删除了: , suggesting that NO₃⁻ promotes PAN formation in the actual atmosphere (Hanst, 1971)

删除了: .



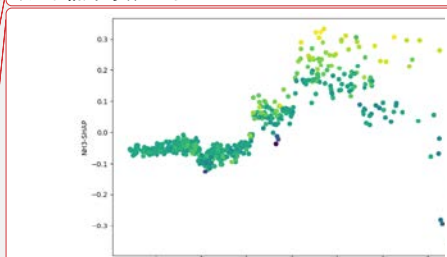
删除了:

设置了格式: 字体: 五号

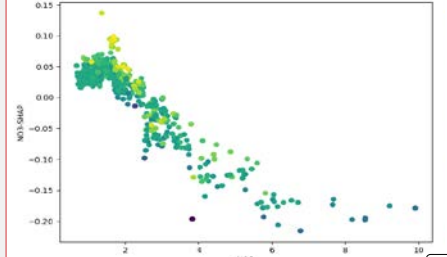
设置了格式: 字体: 五号

设置了格式: 字体: 五号

设置了格式: 字体: 五号



删除了:



删除了: -

删除了: difference between the model simulation values and the observed values (bias)

446 Figure 5 (a) and (b) show the average production and destruction rates of PAN during clean and haze periods, as simulated by
447 OBM without PAN constrained. During the haze period, both the production and destruction rates of PAN are significantly higher
448 than during the clean period. The higher production rate of PAN during the haze period is due to the higher concentration of PAN
449 precursors, while the higher destruction rate is because both the temperature and PAN concentration are higher. Regarding the net
450 production rate, it is also higher during the haze period than during the clean period, which corresponds to the previously observed
451 diurnal variation. From 6:00 to 12:00 during the haze period, the simulated net production rate of PAN is positive, with an average
452 value of 0.19 ppb·h⁻¹. During the clean period, from 6:00 to 12:00, the simulated net production rate of PAN is 0.12 ppb·h⁻¹. The
453 observed diurnal variation of PAN shows that from 6:00 to 12:00, the average net production rates during the haze and clean
454 periods are 0.20 ppb·h⁻¹ (Fig. 2(a)) and 0.09 ppb·h⁻¹ (Fig. 2(b)), respectively. The model-simulated net production rate is close to
455 the observed net production rate, further indicating that the model can simulate PAN well, and also confirming that PAN in summer
456 mainly comes from local production. The net production rate of PAN during the haze period is similar to the summer results in
457 urban areas of the Pearl River Delta (PRD), which is 0.17 ppb·h⁻¹, while the net production rate of PAN during the clean period is
458 similar to the summer results in rural areas of the PRD, which is 0.12 ppb·h⁻¹ (Liu et al., 2024).

459 Figure 5 (c) and (d) show the average production and destruction rates of PAN during clean and haze periods, as simulated by OBM
460 with PAN constrained. The net production rate of PAN is approximately zero at night during both clean and haze periods, while
461 there is a significant difference in the net production rate during the day. During the clean period, the daytime net production rate of
462 PAN is greater than zero, with an average value of 0.19 ppb·h⁻¹. In contrast, during the haze period, the net production rate of PAN
463 is negative from 6 a.m. to 1 p.m., with an average value of -0.47 ppb·h⁻¹, and positive from 2 p.m. to 5 p.m., with an average value
464 of 0.47 ppb·h⁻¹. Previous research has shown that an increase in temperature, an increase in PAN concentration, or a decrease in
465 PAN precursors (including VOCs and NO₂) can cause the net production rate of PAN to change from positive to negative (Liu et al.,
466 2024). We conducted a correlation analysis of the net production rate of PAN with temperature, PAN, VOCs, and NO₂ concentration
467 and found that the net production rate of PAN had the best correlation with PAN concentration (R²=0.1316), showing a significant
468 negative correlation (k=-0.5283) (Fig. S12). Additionally, we also observed that when the net production rate of PAN is negative,
469 the PAN concentration is often very high (Fig. S12). As shown in Fig. 6, we conducted sensitivity experiments by reducing the PAN
470 concentration by 80 %, i.e., 0.2 times the observed value, and found that the simulated net production rate of PAN was positive
471 throughout the observation period. Conversely, when the PAN concentration was increased by 140%, i.e., 2.4 times the observed
472 value, the simulated net production rate of PAN was found to be almost negative throughout the observation period. Besides, we
473 also conducted sensitivity experiments on temperature and found that when simulating winter temperatures, i.e., 0.4 times the
474 observed value, with a temperature range of 9.25-15.29°C, the simulated net production rate of PAN was positive throughout
475 the observation period. Similarly, when simulating spring and autumn temperatures, i.e., 0.6 times the observed value, with a
476 temperature range of 13.87-23.39°C, the simulated net production rate of PAN was also positive throughout the observation period.

删除了: concentration

删除了: S7

删除了: S7

删除了: 5

In conclusion, the simulated net production rate of PAN becomes negative with PAN constrained, further suggesting the existence of an unknown compensatory mechanism.

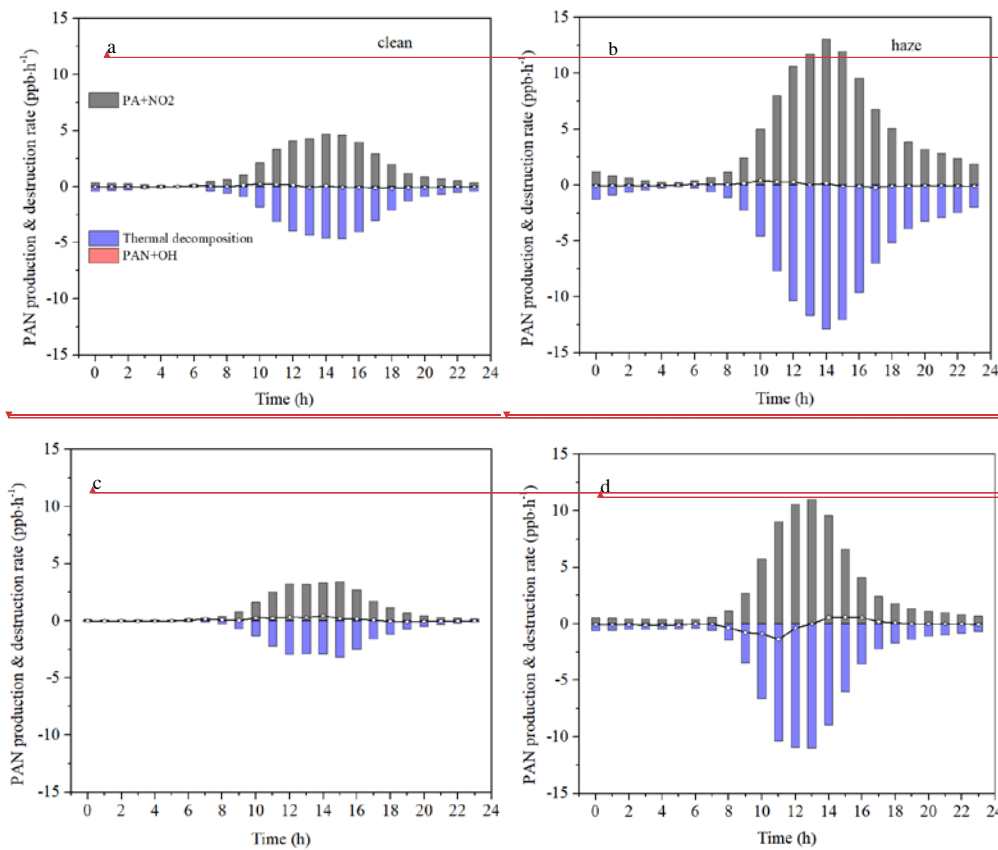
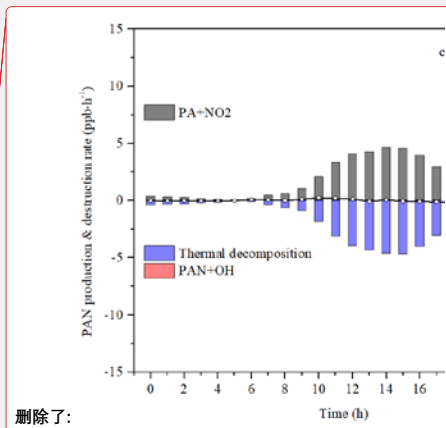
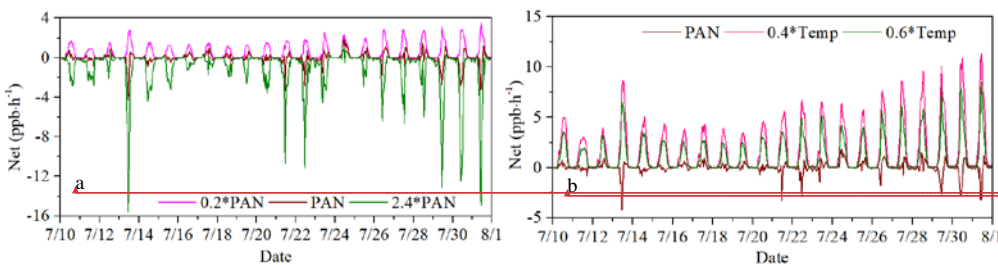
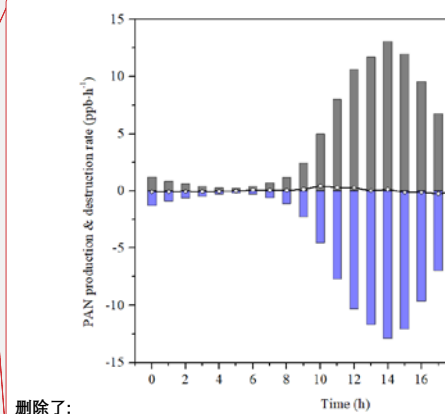


Figure 5. Average diurnal variation of the OBM simulated production, destruction and net rates of PAN during clean (a) and haze (b) without PAN constrained. And average diurnal variation of the OBM simulated production, destruction and net rates of PAN during clean (c) and haze (d) with PAN constrained.

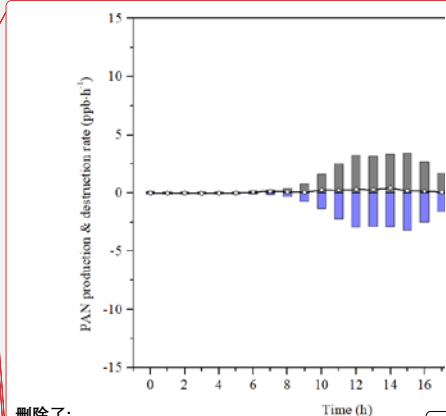


删除了:



删除了:

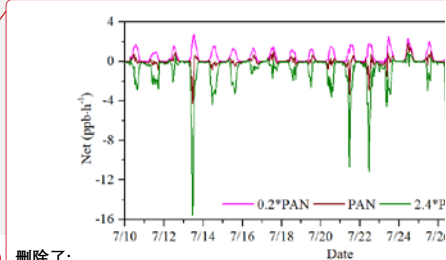
设置了格式: 字体: 五号



删除了:

设置了格式: 字体: 五号

设置了格式: 字体: 五号



删除了:

设置了格式: 字体: 五号

设置了格式: 字体: 五号

505 **Figure 6.** Net PAN production rates simulated by OBM at different PAN concentrations (a) and different temperatures (b).

506
507 PAN is formed when the PA radical reacts with NO₂. Given the swift equilibrium between R2 and R4 at high temperatures, budget
508 analysis of PA's production and consumption pathways are frequently used to detail the mechanisms behind PAN formation (Sun et
509 al., 2020; Liu et al., 2022a; Liu et al., 2024). Figure 7 illustrates the diurnal patterns of the primary production and loss pathways
510 for the PA radical simulated by OBM across different periods. As shown in Fig. 7, during haze days, the rates of PA production and
511 destruction were twice as high as those on clean days. This indicates that radical cycling and photochemical formation were more
512 efficient during haze days, driven by higher temperatures and a greater abundance of precursors (Zeng et al., 2019). The PA radical
513 production rate from PAN thermal decomposition reached its peak at 15:00 (3.22 ppb-h⁻¹) and 13:00 (10.99 ppb-h⁻¹) for clean and
514 haze days, perfectly coinciding with the peak temperature time. In addition, the conversion of PAN into PA radical through thermal
515 decomposition had high exponential correlations with temperature during both haze ($R^2=0.95$) and clean days ($R^2=0.91$) (Fig. S13).
516 Previous laboratory experiments also indicated that the thermal decomposition of PAN is exponentially related to temperature (Cox
517 & Roffey 1977; Senum et al., 1986; Tuazon et al., 1990). The conversion of PAN into PA radical through thermal decomposition
518 during haze days was significantly higher than that during clean days, which was not only enhanced by higher temperature but also
519 maintained by higher PAN concentration during haze days. The thermal decomposition of PAN to PA radical during the day (5:00-
520 18:00 local time) accounted for 68.22 % and 45.59 % during haze and clean days, respectively. The pathways that did not account
521 for the transformation between PA and PAN reached their peak around noon (11:00 local time), coinciding with the highest solar
522 radiation and the most intense photochemical reactions, which has been observed in spring and autumn at the same site (Liu et al.,
523 2022a).

524 Production rates of PA from other pathways related to precursors, including OVOCs, radical cycling, MGLY, and CH₃CHO, showed
525 single-peak patterns around noon, which suggested that the PA radical generated from these pathways was primarily increased by
526 intense solar radiation at noontime (Sun et al., 2020). The average day PA radical production rates from CH₃CHO via reactions with
527 OH and NO₃ were 1.10 and 0.93 ppb-h⁻¹, accounting for 48.85% and 49.35 % (exclude PAN thermal decomposition sources) during
528 haze and clean days, respectively. These percentages were comparable to previous studies in Guangzhou (46 %) (Yuan et al., 2018)
529 and Beijing (34.11-50.19 %) (Xue et al., 2014), suburban site of Chongqing (47.72 %) (Sun et al., 2020). The second production
530 pathway involved MGLY undergoing photolysis and oxidation through reactions with OH and NO₃ (haze: 0.50 ppb-h⁻¹ and clean:
531 0.42 ppb-h⁻¹), contributing to 22.27 % and 22.12 % for haze and clean days, respectively. Subsequently, radical cycling processes—
532 including the decomposition of RO radicals and the reactions of acyl peroxy radicals with NO—were also significant contributors
533 to PA production, accounting for 18.98% on haze days and 19.54% on clean days. PA from the other OVOCs (excluding CH₃CHO,
534 MGLY) via photolysis and oxidation reactions involving OH, NO₃, and O₃, accounted for 9.90 % and 8.99% during haze (0.22
535 ppb-h⁻¹) and clean days (0.17 ppb-h⁻¹). There were no notable differences in the proportions of individual pathways contributing to

删除了: is

删除了: 82

删除了: 77

删除了:

删除了:

删除了: of these four pathways

PA between haze and clean days, indicating comparable pollutant compositions in the atmospheric around IUE (Zeng et al., 2019). In summary, the thermal decomposition of PAN played the dominant role in boosting PA production rates during both clean and haze periods, followed by contributions from CH₃CHO, MGLY, radical cycling, and other OVOCs. The primary contributor to the PA destruction rate was the reaction between PA and NO₂, accounting for 67.72 % and 51.09 % during haze (4.74 ppb-h⁻¹) and clean days (1.76 ppb-h⁻¹), respectively, followed by PA+NO, contributing to 32.28 % and 48.91 % during haze (2.26 ppb-h⁻¹) and clean days (1.69 ppb-h⁻¹), respectively.

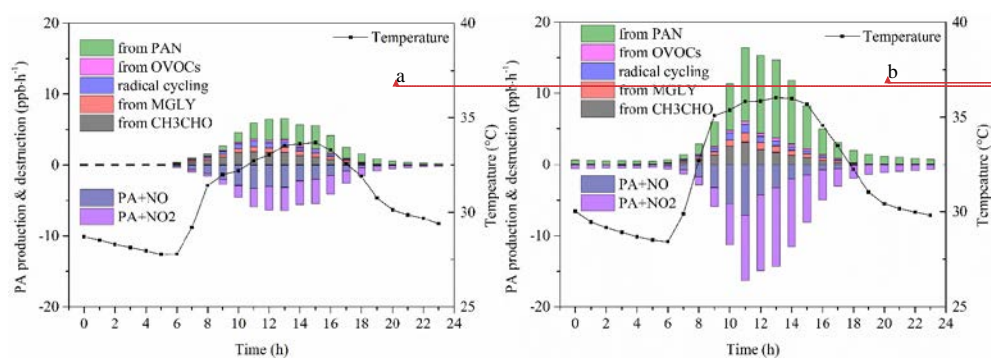


Figure 7. PA radical production and destruction pathways simulated by OBM on (a) clean days and (b) haze days.

3.3 Sensitivity of PAN formation and its impact on the local atmosphere

To determine the principal precursors influencing PAN formation, sensitivity modeling analyses were carried out to investigate how PAN relates to its precursors. The RIR reflects how sensitive PAN formation is to changes in its precursor levels. As shown in Fig. 8 (a), the RIR of NO was negative, ranging from -0.67 to -0.27 (-0.52 ± 0.13) throughout the observation period. However, RIR is positive for other species, with NO₂ (0.50 ± 0.11) and VOCs (0.50 ± 0.15) having the highest RIR, followed by HONO (0.12 ± 0.04) and O₃ (0.10 ± 0.03). Around 50 types of VOCs were classified as alkanes, OVOCs, halogenated hydrocarbons (Halo), alkenes, aromatics (Arom), and isoprene (C₅H₈ representing biogenic hydrocarbons). Among these VOCs, the RIR of alkenes (0.22 ± 0.07) is the highest, followed by C₅H₈ (0.13 ± 0.04) and Arom (0.13 ± 0.04), while OVOCs (0.06 ± 0.01) and Halo (0.05 ± 0.01) have very low RIRs (Fig. 8 (b)). These phenomena indicated that increased NO level would inhibit the production of PAN while increased NO₂, VOCs (especially alkenes, C₅H₈, and Arom), HONO, and O₃ would promote the production of PAN. Because the values of NO and NO₂ RIR are approximately equal but with opposite signs, the RIR for NO_x is almost zero, indicating that the PAN generation at this site is not sensitive to NO_x. Zeng et al. (2019) also observed that NO₂ had a positive effect on PAN formation, while NO had a negative effect, in a suburban area of Hong Kong. This finding aligns with the fact that NO₂ directly contributes to PAN production, whereas NO reduces PA radicals, thereby inhibiting PAN formation. Based on the scenario analysis (Empirical Kinetic Modeling Approach (EKMA)), all data points for the 22 days fell above the ridge line (Fig. 8(c)). A reduction

设置了格式: 下标

删除了: N

删除了:

设置了格式: 字体: 五号

设置了格式: 字体: 五号

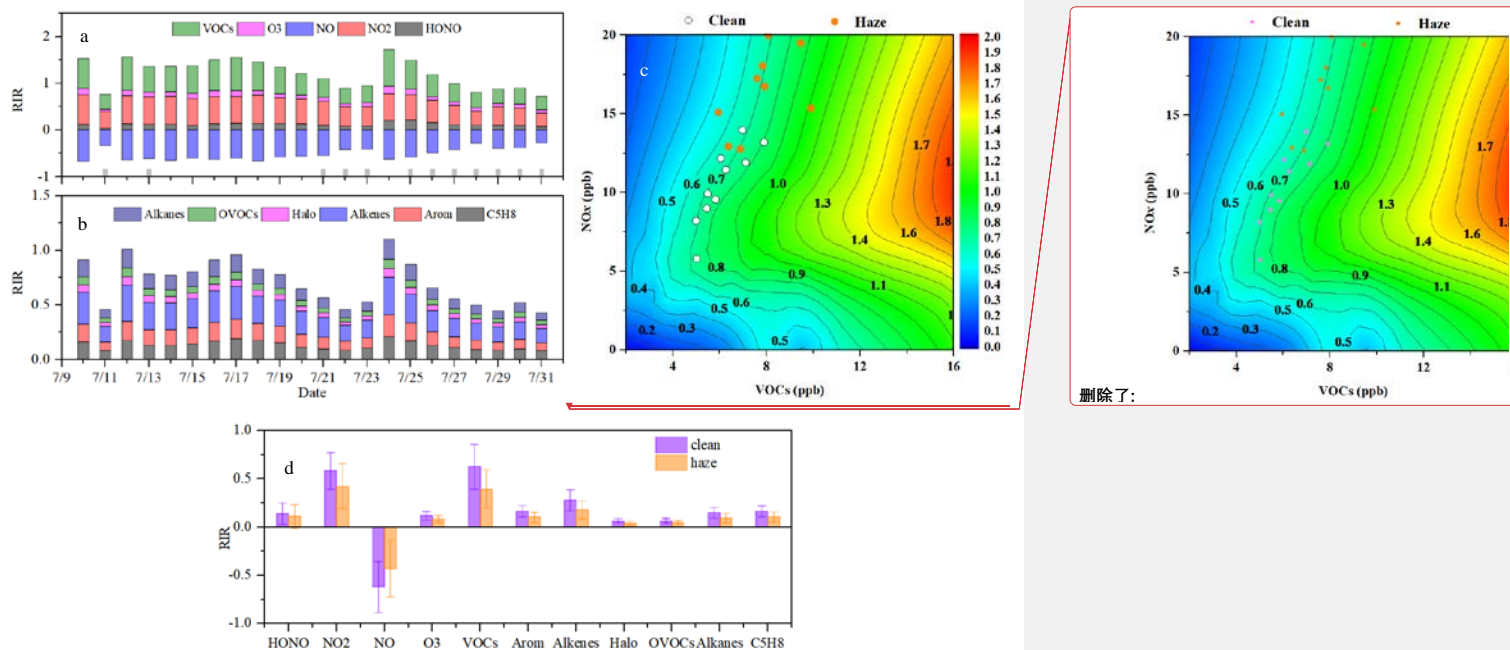
删除了: decreases in NO led to strong negative RIR

设置了格式: 下标

设置了格式: 字体: 非倾斜, 下标

570 in VOCs at these points resulted in lower PAN concentrations, indicating that PAN formation at IUE was influenced by VOCs and
 571 thus VOC-sensitive. Our previous research also found that in this coastal city, PAN generation is limited by VOCs during the
 572 spring and autumn seasons. The difference is that previous studies indicated that reducing NO₂, like reducing NO, also leads to an
 573 increase in PAN concentration in spring and autumn (Liu et al., 2022a). This is because the NO_x concentration in spring and autumn
 574 is significantly higher than in summer, which is consistent with that both NO₂ and NO inhibit the formation of PAN in regions
 575 with high NO_x concentrations (Liu et al., 2024).

576 We divided the RIRs for different species into haze and clean periods and found that the RIRs during clean periods were consistently
 577 higher than those during haze periods (Fig. 8(d)), which indicated that altering the concentrations of these species during clean
 578 periods had a greater impact on PAN formation. The rapid thermal decomposition of PAN at high temperatures is likely the primary
 579 reason. During the haze period, the main source of PA radical was PAN decomposition, which accounted for 68.22%, and the other
 580 sources were smaller than that during the clean period (the source of the PA radical would be demonstrated in the following
 581 paragraph). Therefore, the sensitivity of PAN production to precursors and HONO & O₃ producing OH became lower during the
 582 haze period (Liu et al., 2021b; Liu et al., 2022a).



584 **Figure 8.** These four figures illustrate the RIR of PAN formation to major precursors (a), the impact of different VOCs species (b),
 585 the isopleth diagrams of PAN formation (c), and a comparison of RIRs between clean and polluted periods (d).
 586

587 As shown in Fig. 9, ΔHO₂ and ΔOH are positive for most periods, accounting for 72.16% and 70.83%, respectively, indicating that
 588

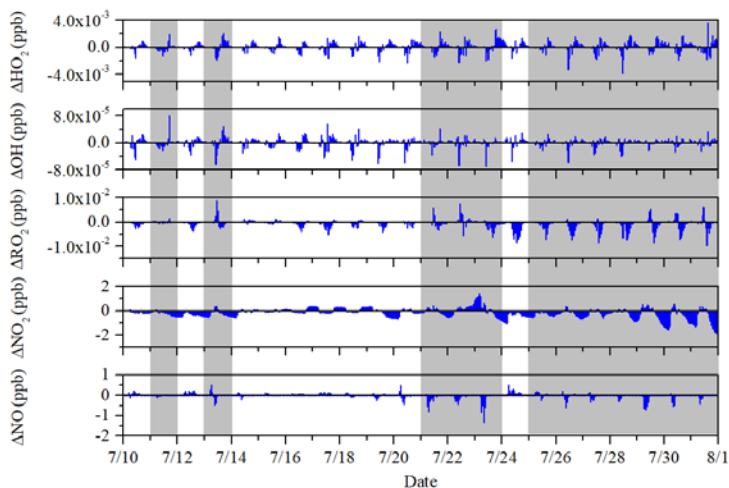
删除了: NO_x

设置了格式: 字体: 非倾斜, 下标

设置了格式: 字体: 非倾斜, 下标

删除了:

591 the PAN mechanism promotes the generation of HO₂ and OH. Over the entire period, ΔHO₂ is 8.43×10⁻⁵ ppb, with no significant
 592 difference between clean and hazy periods, being 8.18×10⁻⁵ ppb and 8.64×10⁻⁵ ppb respectively (Table S1). OH behaves similarly,
 593 with ΔOH being 4.55×10⁻⁷ ppb over the entire period, and also showing no significant difference between clean and hazy periods,
 594 being 4.94×10⁻⁷ ppb and 4.23×10⁻⁷ ppb respectively (Table S1). The increase in simulated OH and HO₂ concentrations suggests that
 595 PAN photochemistry is in favor of radical formation and atmospheric oxidative capacity at this site (Liu et al., 2024). Unlike HO₂
 596 and OH, ΔRO₂ and ΔNO₂ are negative for most periods, accounting for 53.22% and 67.23%, respectively, because PAN formation
 597 uses up PA and NO₂, the reduction in PA leads to a decrease in the amount of RO₂. Over the entire period, ΔRO₂ is -6.4×10⁻⁴ ppb,
 598 with no significant difference between clean and hazy periods, being -6.11×10⁻⁴ ppb and -6.55×10⁻⁴ ppb respectively (Table S1).
 599 The average value of ΔNO₂ during the entire observation period is -0.17 ppb respectively, with significant differences between hazy
 600 and clean periods (Table S1). Specifically, ΔNO₂ is -0.22 during hazy periods and only -0.11 during clean periods, indicating that
 601 the PAN mechanism consumes more NO₂ during hazy periods. Although ΔNO is positive for most periods, accounting for 78.79%,
 602 the overall mean is -0.01, with significant differences between hazy and clean periods (Table S1). ΔNO is -0.05 during hazy periods,
 603 showing an inhibitory effect, while it is 0.03 during clean periods, showing a promoting effect.



604 **Figure 9.** The time series of ΔHO₂, ΔOH, ΔRO₂, ΔNO₂, and ΔNO. The ΔHO₂, ΔOH, ΔRO₂, ΔNO₂, and ΔNO is calculated as the
 605 base scenario with the PAN mechanism minus the scenario without the PAN mechanism.

608 As shown in Fig.10 (a), the PAN mechanism inhibited 85.80% of net O₃ production during the entire observation period, with
 609 inhibition rates (the percentage of negative ΔNet (O₃)) of 83.75% and 87.50% during clean and haze periods, respectively. This
 610 result is consistent with previous spring observations at the same site, where the inhibition rate was 83% (Liu et al., 2022a). The
 611 PAN mechanism mainly inhibits the net O₃ generation by increasing the RO₂+NO₂ reaction (Fig.10(a)), with negligible impact from

- 删除了: 93
- 删除了: enhancing
- 删除了: AOC
- 删除了: ,
- 删除了: , and ΔNO
- 删除了:
- 删除了: s
- 删除了: and ΔNO
- 删除了: are
- 删除了: and -0.01
- 删除了:
- 删除了: Similarly,

- 设置了格式: 字体: 非加粗
- 设置了格式: 下标
- 设置了格式: 下标
- 设置了格式: 下标
- 删除了: The difference of HO₂, OH, RO₂, NO₂, and NO between base scenario with PAN mechanism and scenario without PAN mechanism...
- 删除了: ozone
- 设置了格式: 下标
- 删除了: ozone

other reactions (Fig. S14). As shown in Fig.10(b), the diurnal variation trend indicates that the PAN mechanism's inhibitory effect on O_3 is significantly greater during haze periods than during clean periods. Additionally, regardless of whether it is during haze periods or clean periods, the PAN mechanism's inhibitory effect on O_3 is significantly greater during the day than at night. These phenomena all indicate that the higher the PAN concentration, the more pronounced the inhibitory effect of the PAN mechanism on O_3 (Fig.10(c)). Under the condition of low precursors (including NO_x and VOCs) conditions, competition among these precursors may limit their secondary transformation, thus resulting in inhibition (Liu et al., 2024).

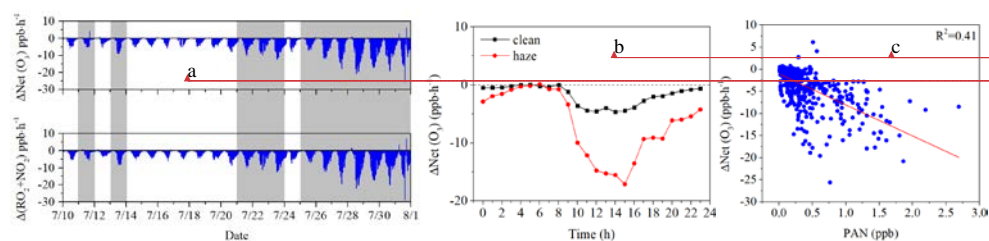


Figure 10. (a) Time series plot of $\Delta\text{Net}(O_3)$ and the reaction of $\Delta(RO_2+NO_2)$. (b) Diurnal variation of $\Delta\text{Net}(O_3)$ during clean and hazy conditions, (c) Correlation between $\Delta\text{Net}(O_3)$ and PAN. $\Delta\text{Net}(O_3)$ and $\Delta(RO_2+NO_2)$ are calculated as the base scenario with the PAN mechanism minus the scenario without the PAN mechanism.

Conclusion

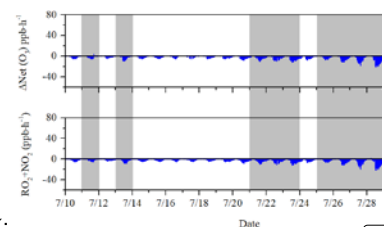
This study thoroughly investigated the summertime PAN formation mechanism and established its connection to haze pollution. In addition to NO and TVOCs, the concentration of all pollutants during the haze period is above twice that during the cleaning period, indicating that the oxidation of NO and TVOCs during the haze period is stronger, which is conducive to the oxidation of NO and TVOCs into secondary pollutants, such as O_3 and PAN. The slopes of linear regression between the daily maximum values of PAN and O_3 were 0.021 ppb/ppb and 0.009 ppb/ppb for clean and hazy condition, respectively, implies that PAN precursors accounted for only a small fraction of the total VOCs, especially for hazy condition. High temperature should be another factor contributing to the lower production efficiency of PAN in the southeast coastal region. During the whole observation period, the IOA=0.75, indicating that the MCM model is well-suited for exploring the photochemical formation of PAN. During the clean period, simulation results were better than during the haze period (R^2 : 0.68 vs. 0.47, slope K: 0.91 vs. 0.75), indicating that some reactions related to PAN generation or destruction might be missing in the MCM during the hazy period. Additionally, the simulated net production rate of PAN becomes negative with PAN constrained. However, the observed increasing in PAN concentrations indicates that the actual net production rate is positive, suggesting that there are additional sources contributing to PAN generation that are not considered in the MCM mechanism. Through XGBoost-SHAP machine learning, and given the significant positive correlation between PAN and NO_3^- ($R=0.37$) at the 0.01 level, and their peak around noon, they likely share a common source. Both RIR and EKMA indicate that PAN formation in this region is VOC-controlled. Controlling emissions of VOCs, particularly alkenes, C_5H_8 ,

删除了: S11...14). As shown in Fig.10(b), the diurnal variation trend indicates that the PAN mechanism's inhibitory effect on O_3 ...is significantly greater during haze than during clean periods. Additionally, regardless of whether it is during haze periods or clean periods, the PAN mechanism's inhibitory effect on O_3 ...is significantly greater during the day than at night. These phenomena all indicate that the higher the PAN concentration, the more pronounced the inhibitory effect of the PAN mechanism on O_3 ...

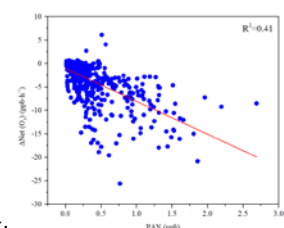
删除了: ,

设置了格式: 字体: 非倾斜, 下标

删除了: secondary formation



删除了:



删除了:

设置了格式: 字体: 五号

设置了格式: 字体: 五号

设置了格式: 字体: 五号

设置了格式: 非上标/ 下标

删除了: 6782 ...8 vs. 0.4708... slope K: 0.9097 ...1 vs. 0.7477...5), indicating that some reactions related to PAN generation or destruction might be missing in the MCM

删除了: this unknown compensatory mechanism may involve NO_3^- promoting PAN formation.

设置了格式

712 and aromatics, would be beneficial for mitigating PAN pollution. The RIR results also show that during the clean period, PAN is
713 more sensitive to changes in various pollutants than during the haze period, highlighting the significant importance of deep emission
714 reductions. PAN presented the promotion effects on OH and HO₂, while inhibited O₃ formation, RO₂, NO and NO₂. This study
715 improves our thorough understanding of PAN photochemistry and offers valuable scientific guidance for the future management of
716 PAN pollution.

717 **Data availability**

718 The observation data at this site are available from the authors upon request.

719 **Authorship Contribution Statement**

720 **Baoye Hu:** Methodology, Formal analysis, Investigation, Data curation, Writing – original draft. **Naihua Chen:** Software, Formal
721 analysis. **Rui Li:** Software, Formal analysis. **Mingqiang Huang:** Software. **Jinsheng Chen:** Funding acquisition, Supervision,
722 Writing - Review & Editing. **Youwei Hong:** Formal analysis. **Lingling Xu:** Investigation. Xiaolong Fan: Investigation. **Mengren**
723 **Li:** Investigation. **Lei Tong:** Investigation. **Qiuping Zheng:** Investigation. **Yuxiang Yang:** Writing - Review & Editing

724 **Competing interests**

725 The authors declare that they have no conflict of interest.

726 **Acknowledgments**

727 This work was supported by the National Natural Science Foundation of China (grant nos. 42305102, U22A20578), Natural Science
728 Foundation of Fujian Province (grant nos. 2023J05179), Natural Science Foundation of Zhangzhou City (grant nos. ZZ2023J07),
729 Fujian Provincial Department of Education (grant nos. JAT210279), the Fund of Minnan Normal University President (grant nos.
730 KJ2021009). This study was funded by Xiamen Atmospheric Environment Observation and Research Station of Fujian Province,
731 and Fujian Key Laboratory of Atmospheric Ozone Pollution Prevention (Institute of Urban Environment, Chinese Academy of
732 Sciences).

733 **Supplementary information**

734 Attached please find supplementary information associated with this article.

删除了:

736
737
738
739
740
741
742
743
744
745
746
747
748
749
750
751
752
753
754
755
756
757
758
759
760
761
762
763
764
765
766

Reference

Behera, S. N., Sharma, M., Aneja, V. P., and Balasubramanian, R.: Ammonia in the atmosphere: a review on emission sources, atmospheric chemistry and deposition on terrestrial bodies, *Environ. Sci. Pollut. Res.*, 20, 8092-8131, 10.1007/s11356-013-2051-9, 2013.

Cox, R. A., & Roffey, M. J. : Thermal decomposition of peroxyacetyl nitrate in the presence of nitric oxide. *Environ. Sci. Tech.*, 11, 900-906. 10.1021/es60132a010. 1977.

Duan, J., Qin, M., Ouyang, B., Fang, W., Li, X., Lu, K., Tang, K., Liang, S., Meng, F., Hu, Z., Xie, P., Liu, W., and Häseler, R.: Development of an incoherent broadband cavity-enhanced absorption spectrometer for in situ measurements of HONO and NO₂, *Atmos. Meas. Tech.*, 11, 4531-4543, 10.5194/amt-11-4531-2018, 2018.

Hong, Z., Li, M., Wang, H., Xu, L., Hong, Y., Chen, J., Chen, J., Zhang, H., Zhang, Y., Wu, X., Hu, B., and Li, M.: Characteristics of atmospheric volatile organic compounds (VOCs) at a mountainous forest site and two urban sites in the southeast of China, *Sci. Total Environ.*, 657, 1491-1500, 10.1016/j.scitotenv.2018.12.132, 2019.

Hu, B., Liu, T., Hong, Y., Xu, L., Li, M., Wu, X., Wang, H., Chen, J., and Chen, J.: Characteristics of peroxyacetyl nitrate (PAN) in a coastal city of southeastern China: Photochemical mechanism and pollution process, *Sci. Total Environ.*, 719, 10.1016/j.scitotenv.2020.137493, 2020.

Hu, B., Wang, Y., Chen, J., Chen, N., Hong, Y., Xu, L., Fan, X., Li, M., and Tong, L.: The observation of atmospheric HONO by wet-rotating-denuder ion chromatograph in a coastal city: Performance and influencing factors, *Environ. Pollut.*, 356, 10.1016/j.envpol.2024.124355, 2024.

Hu, B., Duan, J., Hong, Y., Xu, L., Li, M., Bian, Y., Qin, M., Fang, W., Xie, P., and Chen, J.: Exploration of the atmospheric chemistry of nitrous acid in a coastal city of southeastern China: results from measurements across four seasons, *Atmos. Chem. Phys.*, 22, 371-393, 10.5194/acp-22-371-2022, 2022.

Li, H., Yang, Y., Su, H., Wang, H., Wang, P., and Liao, H.: Ozone ~~pollution in China affected by climate change in a carbon neutral future as predicted by a process-based interpretable machine learning method~~, *Geophys. Res. Lett.*, 51, 10.1029/2024gl109520, 2024.

Lin, Z., Xu, L., Yang, C., Chen, G., Ji, X., Li, L., Zhang, K., Hong, Y., Li, M., Fan, X., Hu, B., Zhang, F., and Chen, J.: Trends of peroxyacetyl nitrate and its impact on ozone over 2018–2022 in urban atmosphere, *Npj Clim. Atmos. Sci.*, 7, 10.1038/s41612-024-00746-7, 2024.

Liu, L., Wang, X., Chen, J., Xue, L., Wang, W., Wen, L., Li, D., and Chen, T.: Understanding unusually high levels of peroxyacetyl nitrate (PAN) in winter in Urban Jinan, China, *J. Environ. Sci.*, 71, 249-260, 10.1016/j.jes.2018.05.015, 2018.

Liu, T., Chen, G., Chen, J., Xu, L., Li, M., Hong, Y., Chen, Y., Ji, X., Yang, C., Chen, Y., Huang, W., Huang, Q., and Wang, H.: Seasonal characteristics of atmospheric peroxyacetyl nitrate (PAN) in a coastal city of Southeast China: Explanatory factors

删除了: Hanst, P. L.: Mechanism of Peroxyacetyl Nitrate Formation, *J. Air Pollut. Control Assoc.*, 21, 269-271, 10.1080/00022470.1971.10469527, 1971.

- 删除了: Pollution
- 删除了: Affected
- 删除了: Climate
- 删除了: Change
- 删除了: Carbon
- 删除了: Neutral
- 删除了: Future
- 删除了: Predicted
- 删除了: Process
- 删除了: Based
- 删除了: Interpretable
- 删除了: Machine
- 删除了: Learning
- 删除了: Method

784
785
786
787
788
789
790
791
792
793
794
795
796
797
798
799
800
801
802
803
804
805
806
807
808
809
810
811
812
813
814

and photochemical effects, *Atmos. Chem. Phys.*, 22, 4339-4353, 10.5194/acp-22-4339-2022, 2022a.

[Liu, T., Hong, Y., Li, M., Xu, L., Chen, J., Bian, Y., Yang, C., Dan, Y., Zhang, Y., Xue, L., Zhao, M., Huang, Z., and Wang, H.: Atmospheric oxidation capacity and ozone pollution mechanism in a coastal city of southeastern China: analysis of a typical photochemical episode by an observation-based model, *Atmos. Chem. Phys.*, 22, 2173-2190, 10.5194/acp-22-2173-2022, 2022b.](#)

Liu, T., Wang, Y., Cai, H., Wang, H., Zhang, C., Chen, J., Dai, Y., Zhao, W., Li, J., Gong, D., Chen, D., Zhai, Y., Zhou, Y., Liao, T., and Wang, B.: Complexities of peroxyacetyl nitrate photochemistry and its control strategies in contrasting environments in the Pearl River Delta region, *Npj Clim. Atmos. Sci.*, 7, 10.1038/s41612-024-00669-3, 2024.

Liu, X., Guo, H., Zeng, L., Lyu, X., Wang, Y., Zeren, Y., Yang, J., Zhang, L., Zhao, S., Li, J., and Zhang, G.: Photochemical ozone pollution in five Chinese megacities in summer 2018, *Sci. Total Environ.*, 801, 149603, 10.1016/j.scitotenv.2021.149603, 2021a.

Liu, Y., Shen, H., Mu, J., Li, H., Chen, T., Yang, J., Jiang, Y., Zhu, Y., Meng, H., Dong, C., Wang, W., and Xue, L.: Formation of peroxyacetyl nitrate (PAN) and its impact on ozone production in the coastal atmosphere of Qingdao, North China, *Sci. Total Environ.*, 778, 10.1016/j.scitotenv.2021.146265, 2021b.

Lu, X., Zhang, L., Wang, X., Gao, M., Li, K., Zhang, Y., Yue, X., and Zhang, Y.: Rapid Increases in Warm-Season Surface Ozone and Resulting Health Impact in China Since 2013, *Environ. Sci. Tech. Lett.*, 7, 240-247, 10.1021/acs.estlett.0c00171, 2020.

Marley, N. A., Gaffney, J. S., Ramos-Villegas, R., and , B. C. G.: Comparison of measurements of peroxyacetyl nitrates and primary carbonaceous aerosol concentrations in Mexico City determined in 1997 and 2003, *Atmos. Chem. Phys.*, 7, 2277-2285, 2007a.

Marley, N. A., Gaffney, J. S., Ramos-Villegas, R., and Gonzalez, B. C.: Comparison of measurements of peroxyacetyl nitrates and primary carbonaceous aerosol concentrations in Mexico City determined in 1997 and 2003, *Atmos. Chem. Phys.*, 7, 2277-2285, 2007b.

[Pratap, V., Carlton, A. G., Christiansen, A. E., and Hennigan, C. J.: Partitioning of ambient organic gases to inorganic salt solutions: influence of salt identity, ionic strength, and pH, *Geophys. Res. Lett.*, 48, 10.1029/2021gl095247, 2021.](#)

Roberts, J. M., Flocke, F., Stroud, C. A., Hereid, D., Williams, E., Fehsenfeld, F., Brune, W., Martinez, M., and Harder, H.: Ground-based measurements of peroxyacetyl nitric anhydrides (PANs) during the 1999 Southern Oxidants Study Nashville Intensive, *J Geophys Res-Atmos*, 107, ACH 1-1-ACH 1-10, 10.1029/2001jd000947, 2002.

[Senum, G. I., Fajer, R., & Gaffney, J. S. Fourier transform infrared spectroscopic study of the thermal stability of peroxyacetyl nitrate, *J. Phys. Chem.*, 90, 152-156, 10.1021/j100273a034, 1986.](#)

Sun, M., Cui, J. n., Zhao, X., and Zhang, J.: Impacts of precursors on peroxyacetyl nitrate (PAN) and relative formation of PAN to ozone in a southwestern megacity of China, *Atmos. Environ.*, 231, 10.1016/j.atmosenv.2020.117542, 2020.

Sun, M., Zhou, Y., Wang, Y., Qiao, X., Wang, J., and Zhang, J.: Heterogeneous ~~reaction of peroxyacetyl nitrate on real-world~~ PM_{2.5}

- 删除了: Reaction
- 删除了: Peroxyacetyl
- 删除了: Nitrate
- 删除了: Real
- 删除了: World

820 [aerosols: Kinetics, influencing Factors, and atmospheric implications](#), Environ. Sci. Tech., 56, 9325-9334,
821 10.1021/acs.est.2c03050, 2022.

822 Taylor, O. C.: Importance of peroxyacetyl nitrate (PAN) as a phytotoxic air pollutant, J. Air Pollut. Control Assoc., 19, 347-351,
823 10.1080/00022470.1969.10466498, 1969.

824 [Tuazon, E. C., Carter, W. P., & Atkinson, R.: Thermal decomposition of peroxyacetyl nitrate and reactions of acetyl peroxy radicals
825 with nitric oxide and nitrogen dioxide over the temperature range 283-313 K. J. Phys. Chem., 95, 2434-2437,
826 10.1021/j100159a059, 1991.](#)

827 Wang, B., Shao, M., Roberts, J. M., Yang, G., Yang, F., Hu, M., Zeng, L., Zhang, Y., and Zhang, J.: Ground-based on-line
828 measurements of peroxyacetyl nitrate (PAN) and peroxypropionyl nitrate (PPN) in the Pearl River Delta, China. , Int. J.
829 Environ. Anal. Chem., 90, 548–559, 10.1080/03067310903194972, 2010.

830 Wang, H., Lyu, X., Guo, H., Wang, Y., Zou, S., Ling, Z., Wang, X., Jiang, F., Zeren, Y., Pan, W., Huang, X., and Shen, J.: Ozone
831 pollution around a coastal region of South China Sea: interaction between marine and continental air, Atmos. Chem. Phys., 18,
832 4277-4295, 10.5194/acp-18-4277-2018, 2018.

833 Wang, Y., Liu, T., Gong, D., Wang, H., Guo, H., Liao, M., Deng, S., Cai, H., and Wang, B.: Anthropogenic [pollutants induce changes
834 in peroxyacetyl nitrate formation intensity and pathways in a mountainous background atmosphere in southern](#) China, Environ.
835 Sci. Tech., 10.1021/acs.est.2c02845, 2023.

836 Wu, X., Xu, L., Hong, Y., Chen, J., Qiu, Y., Hu, B., Hong, Z., Zhang, Y., Liu, T., Chen, Y., Bian, Y., Zhao, G., Chen, J., and Li, M.:
837 The air pollution governed by subtropical high in a coastal city in Southeast China: Formation processes and influencing
838 mechanisms, Sci. Total Environ., 692, 1135-1145, 10.1016/j.scitotenv.2019.07.341, 2019.

839 Xu, W., Zhang, G., Wang, Y., Tong, S., Zhang, W., Ma, Z., Lin, W., Kuang, Y., Yin, L., and Xu, X.: Aerosol [promotes peroxyacetyl
840 nitrate formation during winter](#) in the North China Plain, Environ. Sci. Technol., 55, 3568-3581, 10.1021/acs.est.0c08157, 2021.

841 Xu, X., Zhang, H., Lin, W., Wang, Y., Xu, W., and Jia, S.: First simultaneous measurements of peroxyacetyl nitrate (PAN) and ozone
842 at Nam Co in the central Tibetan Plateau: impacts from the PBL evolution and transport processes, Atmos. Chem. Phys., 18,
843 5199-5217, 10.5194/acp-18-5199-2018, 2018.

844 Xu, Z., Xue, L., Wang, T., Xia, T., Gao, Y., Louie, P. K. K., and Luk, C. W. Y.: Measurements of [peroxyacetyl nitrate at a background
845 site](#) in the Pearl River Delta [region: production efficiency and regional transport](#), Aerosol Air Qual. Res., 15, 833-841,
846 10.4209/aaqr.2014.11.0275, 2015.

847 Xue, L., Wang, T., Wang, X., Blake, D. R., Gao, J., Nie, W., Gao, R., Gao, X., Xu, Z., Ding, A., Huang, Y., Lee, S., Chen, Y., Wang,
848 S., Chai, F., Zhang, Q., and Wang, W.: On the use of an explicit chemical mechanism to dissect peroxy acetyl nitrate formation,
849 Environ. Pollut., 195, 39-47, 10.1016/j.envpol.2014.08.005, 2014.

850 Xue, L. K., Wang, T., Guo, H., Blake, D. R., Tang, J., and Zhang, X. C.: Sources and photochemistry of volatile organic compounds

删除了: Aerosols

删除了: Influencing

删除了: Atmospheric

删除了: Implications

删除了: Pollutants

删除了: Induce

删除了: Changes

删除了: Peroxyacetyl

删除了: Nitrate

删除了: Formation

删除了: Intensity

删除了: Pathways

删除了: Mountainous

删除了: Background

删除了: Atmosphere

删除了: Southern

删除了: Promotes

删除了: Peroxyacetyl

删除了: Nitrate

删除了: Formation

删除了: During

删除了: Winter

删除了: Peroxyacetyl

删除了: Nitrate

删除了: Background

删除了: Site

删除了: Region

删除了: Production

删除了: Efficiency

删除了: Regional

删除了: Transport

882 in the remote atmosphere of western China: results from the Mt. Waliguan Observatory, Atmos. Chem. Phys., 13, 8551-8567,
883 10.5194/acp-13-8551-2013, 2013.

884 Yang, X., Wu, K., Wang, H., Liu, Y., Gu, S., Lu, Y., Zhang, X., Hu, Y., Ou, Y., Wang, S., and Wang, Z.: Summertime ozone pollution
885 in Sichuan Basin, China: Meteorological conditions, sources and process analysis, Atmos. Environ., 226,
886 10.1016/j.atmosenv.2020.117392, 2020.

887 Ye, C., Zhang, N., Gao, H., and Zhou, X.: Photolysis of ~~particulate nitrate~~ as a ~~source~~ of HONO and NO_x, Environ. Sci. Technol.,
888 51, 6849-6856, 10.1021/acs.est.7b00387, 2017.

889 Yuan, J., Ling, Z., Wang, Z., Lu, X., Fan, S., He, Z., Guo, H., Wang, X., and Wang, N.: PAN-~~precursor relationship and process~~
890 ~~analysis of PAN variations~~ in the Pearl River Delta ~~region~~, Atmos., 9, 10.3390/atmos9100372, 2018.

891 Yukihiro, M., Hiramatsu, T., Bouteau, F., Kadono, T., and Kawano, T.: Peroxyacetyl nitrate-induced oxidative and calcium signaling
892 events leading to cell death in ozone-sensitive tobacco cell-line, Plant Signal Behav., 7, 113-120, 10.4161/psb.7.1.18376, 2012.

893 Zeng, L., Fan, G. J., Lyu, X., Guo, H., Wang, J. L., and Yao, D.: Atmospheric fate of peroxyacetyl nitrate in suburban Hong Kong
894 and its impact on local ozone pollution, Environ. Pollut., 252, 1910-1919, 10.1016/j.envpol.2019.06.004, 2019.

895 Zhai, S., Jacob, D. J., Franco, B., Clarisse, L., Coheur, P., Shah, V., Bates, K. H., Lin, H., Dang, R., Sulprizio, M. P., Huey, L. G.,
896 Moore, F. L., Jaffe, D. A., and Liao, H.: Transpacific ~~transport of Asian peroxyacetyl nitrate (PAN) observed from satellite:~~
897 ~~implications for ozone~~, Environ. Sci. Tech., 58, 9760-9769, 10.1021/acs.est.4c01980, 2024.

898 Zhang, G., Mu, Y., Zhou, L., Zhang, C., Zhang, Y., Liu, J., Fang, S., and Yao, B.: Summertime distributions of peroxyacetyl nitrate
899 (PAN) and peroxypropionyl nitrate (PPN) in Beijing: Understanding the sources and major sink of PAN, Atmos. Environ., 103,
900 289-296, 10.1016/j.atmosenv.2014.12.035, 2015.

901 Zhang, J., Guo, Y., Qu, Y., Chen, Y., Yu, R., Xue, C., Yang, R., Zhang, Q., Liu, X., Mu, Y., Wang, J., Ye, C., Zhao, H., Sun, Q., Wang,
902 Z., and An, J.: Effect of potential HONO sources on peroxyacetyl nitrate (PAN) formation in eastern China in winter, J. Environ.
903 Sci. (China), 94, 81-87, 10.1016/j.jes.2020.03.039, 2020.

904 Zhang, J. M., Wang, T., Ding, A. J., Zhou, X. H., Xue, L. K., Poon, C. N., Wu, W. S., Gao, J., Zuo, H. C., Chen, J. M., Zhang, X.
905 C., and Fan, S. J.: Continuous measurement of peroxyacetyl nitrate (PAN) in suburban and remote areas of western China,
906 Atmos. Environ., 43, 228-237, 10.1016/j.atmosenv.2008.09.070, 2009.

907 Zhu, J., Wang, S., Wang, H., Jing, S., Lou, S., Saiz-Lopez, A., and Zhou, B.: Observationally constrained modeling of atmospheric
908 oxidation capacity and photochemical reactivity in Shanghai, China, Atmos. Chem. Phys., 20, 1217-1232, 10.5194/acp-20-
909 1217-2020, 2020.

910
911

- 删除了: Particulate
- 删除了: Nitrate
- 删除了: Source
- 设置了格式: 字体: 非倾斜, 下标
- 删除了: Precursor
- 删除了: Relationship
- 删除了: Process
- 删除了: Analysis
- 删除了: Variations
- 删除了: Region
- 删除了: Transport
- 删除了: Asian
- 删除了: Peroxyacetyl
- 删除了: Nitrate
- 删除了: Observed
- 删除了: Satellite
- 删除了: Implications
- 删除了: Ozone